PERGAMON

International Journal of Heat and Mass Transfer 42 (1999) 4005–4016

International Journal of HEAT and MASS TRANSFER

www.elsevier.com/locate/ijhmt

Detailed heat transfer characteristic comparison in straight and 90-deg turned trapezoidal ducts with pin-fin arrays

Jenn-Jiang Hwang*, Chau-Chin Lui

Department of Mechanical Engineering, Chung-Hua University, Hsinchu, Taiwan 300, ROC

Received 6 July 1998; received in revised form 7 January 1999

Abstract

Comparison of endwall heat transfer and pressure drop characteristics is made between the pin-fin trapezoidal ducts with straight and lateral outlet flows. The effect of pin arrangement for the ducts of different-directional outlet flows is also examined. A transient liquid crystal method is used to measure the detailed heat transfer coefficients on the endwall surfaces. It is found that in the straight trapezoidal duct, the local heat transfer coefficient decreases along the spanwise direction from the long sidewall to the short sidewall. In addition, the staggered pin array produces relatively uniform and higher local heat transfer than the in-line pin array. As the flow turns 90° out of the trapezoidal duct, the pin arrangement affects insignificantly the local and endwall-averaged heat transfer. Results further show that the 90° turned trapezoidal ducts inserted with either staggered or in-line pin array perform the best endwall-averaged heat transfer and, meanwhile, pay the largest pressure-drop penalty. The straight trapezoidal duct with in-line pin array, however, has the lowest endwall-averaged heat transfer coefficients as well as the pressure-drop coefficients.

1. Introduction

Fluid flow associated with heat transfer in a fin-array duct has been a subject of extensive research in the past two decades because of its significance in a wide variety of industry applications. As depicted in Fig. 1, pin fins are usually inserted into the internal cooling cavities near the trailing edge of the turbine blade to augment the heat transfer. This device enables the blade to be operated in a firing temperature without failure, and thus improves thermal efficiency and power output.

There have been many experimental investigations and the theoretical analyses on the heat transfer characteristics in pin-fin ducts. VanFossen [1] conducted an experimental study to compare the overall heat transfer coefficients in *rectangular* ducts with staggered arrays of short and long pin fins. The results showed that the short pin fins performed a better overall heat transfer than the long pin fins. Metzger et al. [2] studied experimentally the local heat transfer variation in a *rectangular* duct with a staggered short pin array. They found that the local heat transfer increased in the first few rows, reached a peak value and then slowly decreased to a fully developed value. They further developed heat transfer correlations in terms of the Reynolds number for two different pin configurations. Later, Metzger and Haley [3] experimentally compared the endwall heat transfer to the overall pin array heat transfer in *rectangular* ducts inserted with a staggered pin array. They used the thermally nonactive (wooden) pins and calculated the heat transfer based on the exposed endwall surface area only. It was found

* Corresponding author. Tel.: +886-35-374281; fax: +886-35-373771.

E-mail address: jjhwang@chu.edu.tw (J.J. Hwang)

0017-9310/99/$ - see front matter
PII: S0017-9310(99)00056-3

Nomenclature

A_c	cross sectional area at the trapezoidal duct inlet (m^2)
c_p	specific heat at constant pressure (kJ kg^{-1} K^{-1})
De	equivalent hydraulic diameter at the test section inlet, $4A_c/P_c$ (m)
d	pin diameter, Fig. 3 (m)
G	total mass flux (kg m^{-2} s^{-1})
H_1	height of the long sidewall of the trapezoidal duct, Fig. 3 (m)
H_2	height of the short sidewall of the trapezoidal duct, Fig. 3 (m)
h	heat transfer coefficient (kW m^{-2} K^{-1})
K_L	pressure-drop coefficient, $2\Delta P/(G^2/\rho)$
k	thermal conductivity of the endwall material (W m^{-1} K^{-1})
k_f	air thermal conductivity (W m^{-1} K^{-1})
L	endwall length (along streamwise direction), Fig. 3 (m)
l	fin length (or height) (m)
M	pin column index, Fig. 8
N	pin row index, Fig. 8
Nu	local Nusselt number, $h\ De/k_f$
Nu_s	Nusselt number for fully developed smooth pipe flows, i.e., $Nu_s = 0.023 Re^{0.8} Pr^{0.3}$
$\overline{Nu}$	area-averaged Nusselt number of the endwall
$\overline{Nu}_R$	regionally area-averaged Nusselt number
P_c	peripheral length of the trapezoidal duct
Pr	Prandtl number
ΔP	pressure drop across the test section (kPa)
Re	Reynolds number, $G \times De/\mu$
S_x	longitudinal spacing between the pins, Fig. 3 (m)
S_y	transverse spacing between the pins, Fig. 3 (m)
T_m	mainstream temperature (K)
T_i	initial wall temperature (K)
T_w	wall temperature (K)
t	time (s)
W	width of the endwall plate, Fig. 3 (m)
X	streamwise coordinate with respect to the straight duct, Fig. 2
Y	spanwise coordinate with respect to the straight duct, Fig. 2
z	distance normal to the endwall

Greek symbols

α	thermal diffusivity of the endwall material (m^2 s^{-1})
ρ	air density (kg m^{-3})
μ	viscosity of the air (kg s^{-1} m^{-1})
τ_j	time step

Subscripts

b	bulk mean
i	initial
m	mainstream
s	smooth
w	wall

that the endwall heat transfer coefficient had almost the same level as the combined pin-endwall average. Metzger et al. [4] further experimentally investigated the effect of orientation of flattened pins with respect to the main flow direction on the heat transfer and pressure drops in pin-fin *rectangular* channels. Their results showed that varying the pin orientation may increase the heat transfer and, meanwhile, reduce the pressure drop. Extending the study of VanFossen [1], Brigham and VanFossen [5] investigated the effect of the pin length on the array-averaged heat transfer. Their results showed that for a pin length-to-diameter ratio less than two, the array-averaged heat transfer was not affected by the pin length; while, as a pin length-to-diameter ratio was larger than two, the heat transfer increased significantly with increasing the pin length-to-diameter ratio. Lau et al. [6] employed the mass transfer sublimation technique to measure the local endwall heat/mass transfer coefficients in *rectangular* channels with in-line and staggered pin arrays. Overall and row-averaged heat/mass transfer coefficients were compared well with the previous published data [2]. Recently, Chyu [7], also using a mass transfer sublimating technique, evaluated the effects of fillets at the cylinder-endwall junction and the influence of array geometry on the endwall heat transfer in *rectangular* ducts.

Owing to the aerodynamic consideration, as shown in Fig. 1, the trailing edge of the blade is demanded to be a small wedge profile. Therefore, the cooling cavities in this region should be trapezoidal in the cross-sectional shape [8]. In addition, the coolant from the blade base either turns laterally and then is ejected from blade-tip slots or passes through the pin-fin duct and then exits from the slots along the blade trailing edges. However, the related studies, as noted above, are mostly for pin-fin *rectangular* ducts with straight outlet flow, and so far have not considered the local

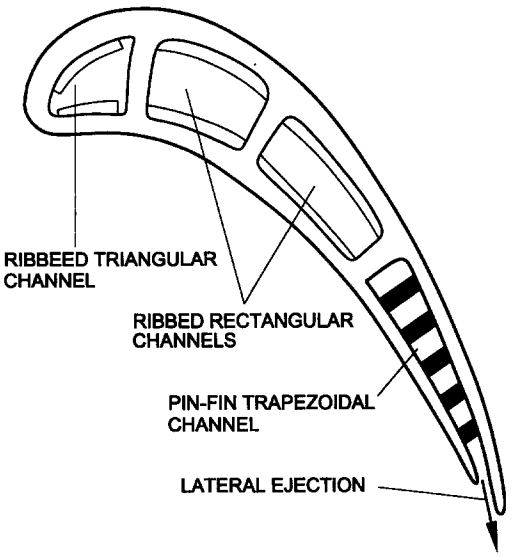

Fig. 1. Cross-sectional view of the modern internally cooled turbine blade.

heat transfer and pressure-drop characteristics in pin-fin *trapezoidal* ducts with straight outlet flow, let alone those in pin-fin trapezoidal ducts with lateral outlet flow. This motivates the present study to investigate experimentally the effect of the outlet flow direction on the heat transfer and pressure drop characteristics in a pin-fin trapezoidal duct. Other parametric studies include the pin configurations (in-line and staggered), and the flow Reynolds numbers ($7000 \leqq Re \leqq 53{,}000$). Changing of the cooling-cavity shape from rectangular to trapezoidal may arouse several interesting factors that influence the heat transfer and pressure drop characteristics. First, due to the effect of duct-area variance along the spanwise direction of the trapezoidal duct, the local heat transfer coefficients distributed on the endwall should be different from those of a symmetrically rectangular geometry. Then, pin fins spanning the distance between two principal walls of the trapezoidal passage are different in length. The heat transfer and pressure drop characteristics in such a kind of duct should be different from those in rectangular ducts with uniform length of pin. Moreover, when the main flow turns laterally out of the pin-fin trapezoidal duct (Fig. 1), not only the flow turning effect but also the variation in the apparent duct throughflow area would affect the forced-convection phenomena. All these have never been studied previously, and will be discussed in the present study.

To resolve the highly localized heat transfer distributions mentioned above, a transient liquid-crystal technique is employed to measure the local heat transfer on the endwall surfaces. The transient liquid-crystal technique used in the present study is similar to Hwang and Cheng [9]. Thin coating are sprayed directly on the endwall of the pin-fin duct, and observed during a transient test with an automated computer vision and data acquisition system. This transient technique using liquid crystals is not only full-surface measurement in characteristic that cannot be achieved using multiple thermocouples, but also can be applied to complex geometry. Moreover, the complicated work in quantifying the heat losses during the steady-state heat transfer experiments is not required by using the present transient technique. The detailed distributions of heat transfer coefficient that are provided by the present work could afford a better understanding of the endwall heat transfer enhancement by pin fins in a trapezoidal duct. They could also provide

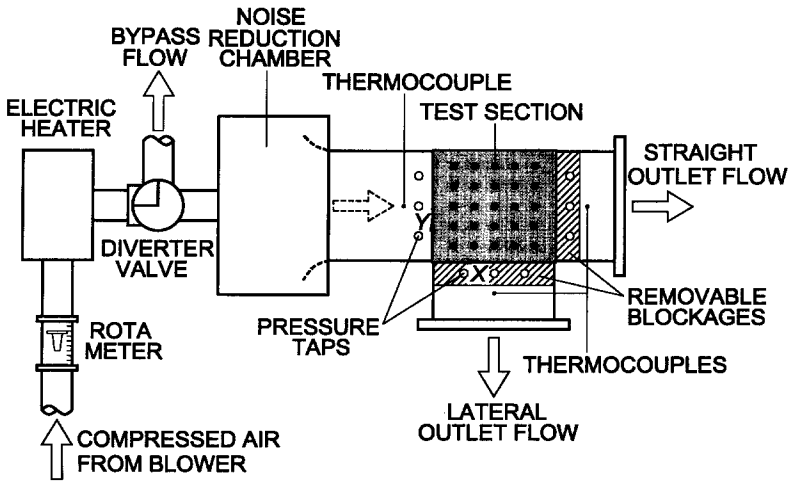

Fig. 2. Schematic drawing of the experimental apparatus.

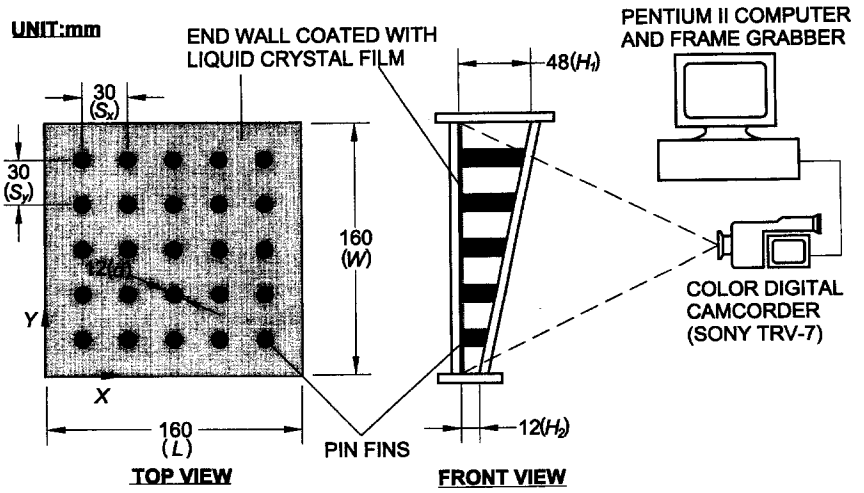

Fig. 3. Dimensions of the pin-fin trapezoidal duct and the image processing system.

a reference of computational-fluid-dynamic-based studies relating to the pin-fin-duct transfer.

2. Experimental apparatus and procedure

2.1. Apparatus

The experimental apparatus shown schematically in Figs. 2 and 3 consists of a blowing-type flow circuit, the test section, and an image-processing system. They are described separately as follows.

Air compressed by a 5-hp blower passes through a rotameter that measures the volume flow rate of the air. It is then ducted into an electric heater to be heated to a required temperature. The hot air from the heater subsequently passes across a noise-reduction chamber and the entrance section (1200 mm in length), and then flows into the test section. Finally, the air exits either laterally or from the straight outlet to the outside of the building via an exhaust system. The test section, as shown in Fig. 3, has a trapezoidal cross section. The entire test section, including the pin fins, is made of Plexiglas®. The endwall sprayed with a thin liquid-crystal film has a square area of 160 × 160 mm (L by W). The long (H_1) and short (H_2) sides of the test section are 48 and 12 mm in height, respectively. That is the height ratio of the long-to-short sides of the trapezoidal test section is 4:1. Either the straight exit or the short side of the test section is blocked by a

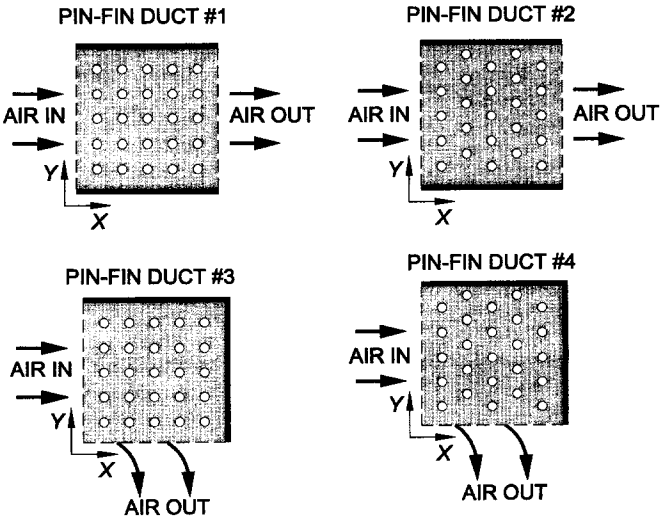

Fig. 4. Four kinds of pin-fin trapezoidal ducts investigated.

Table 1
Test duct configurations

Duct No.	Pin arrangement	Pin number	Straight exit	Lateral exit
1	In line	5 × 5	Open	Blocked
2	Staggered	5 × 5	Open	Blocked
3	In line	5 × 5	Blocked	Open
4	Staggered	5 × 5	Blocked	Open

Plexiglas® barrier. The barrier is screwed in place from the top and bottom walls of the channel rather than attached permanently to the test section. The circular pins of 12 mm in diameter (d) span the distance between two principal duct walls. They have different lengths from $1.3 \leqq l/d \leqq 3.6$ depending on the location within the trapezoidal duct. The pin spacings along the longitude and transverse directions are the same, i.e., $S_x = S_y = 30$ mm. Note that all pins as well as the sidewalls stand vertically on the endwall. The assembly is sealed from the air leakage with petroleum jelly. As shown in Fig. 2, three thermocouple rakes are located at the duct inlet, the straight outlet, and the lateral outlet, respectively, to measure the mainstream temperatures. The time-dependent temperatures are recorded by a data logger (YOKOGAWA, AR 1100A). In addition, the entrance and two exits of the test section are respectively installed with three pressure taps for the static-pressure measurement. They are connected to a micro-differential transducer and a conditioner to amplify the pressure signals which are subsequently transferred to a digital readout.

The image-processing system includes a digital color camcorder (camera + image recorder, SONY DCR-TRV7), a frame grabber card, and a Pentium II personal computer. The camcorder is focused on the liquid-crystal-coated surfaces to view and record their color change during the transient test. The frame grabber interface is programmed to analyze the color change using image-processing software. The software analyzes the picture frame-by-frame and simultaneously records the time lapse of the liquid crystals from colorless to green during the transient test.

Four pin-fin trapezoidal ducts are tested in the present work. As shown in Fig. 4 and Table 1, two of them are inserted with in-line pins (duct Nos 1 and 3), and the remaining two are inserted with staggered pins (not an equilateral triangular array, duct Nos 2 and 4). As for the duct outlet conditions, duct Nos 1 and 2 have a straight outlet flow (referred to as 'straight trapezoidal ducts'), while duct Nos 3 and 4 have a lateral outlet flow (referred to as 'turned trapezoidal ducts').

2.2. Experimental procedure

The test section is assembled after spraying the liquid crystal (Hallcrest, BW/R38C5W/C17-10) uniformly on the endwall surface. The camcorder is set up and focused on the endwall surface. Each test run is thermal transient, initiated by suddenly exposing the hot air to the test section, which results in a color change of the surface coatings. Before the test run, the hot air bypasses the test section so that the endwall remains at the laboratory ambient temperature. The valve keeps in the diverted position until a required mainstream temperature has been achieved in the diversion of the flow loop. Then the valve turns to route the hot air into the test section and, simultaneously, the recorder is switched on to record the mainstream temperature history. The image processing system records the transition time for the color change to green (39°C), and transfers the data into a matrix of time of the color change over the entire surface. The time and temperature data are entered into a computer program to obtain the local heat transfer coefficient.

2.3. Heat transfer theory

The local heat transfer coefficient over the test surface can be obtained by assuming one-dimensional transient conduction over a semi-infinite solid. The one-dimensional transient conduction, the initial condition, and boundary conditions on the liquid crystal coated surface are

$$\begin{aligned} k\frac{\partial^2 T}{\partial z^2} &= \rho c_p \frac{\partial T}{\partial t} \\ &\text{as } t = 0,\ T = T_i; \\ \text{as } t > 0,\ k\frac{\partial T}{\partial z} &= h(T_w - T_m) \\ &\text{at } z = 0; \quad T = T_i, \text{ as } z \to \infty \end{aligned} \tag{1}$$

The surface temperature response to the equation above is shown as:

$$\frac{T_w - T_i}{T_m - T_i} = 1 - \exp\left(\frac{h^2 \alpha t}{k^2}\right) \times \operatorname{erfc}\left(\frac{h\sqrt{\alpha t}}{k}\right) \tag{2}$$

The heat transfer coefficient h can be calculated from the above equation, by knowing the wall temperature (T_w) the initial surface temperature (T_i), the oncoming mainstream temperature (T_m), and the corresponding time (t) required to change the coated-surface color to green at any location. The time required for the color change in a typical run is about 15–90 s depending on the location, mainstream temperature, and throughflow rate. This testing time is so short that the heat flow can hardly penetrate the depth of the acrylic. Therefore, the assumption of the semi-infinite solid on

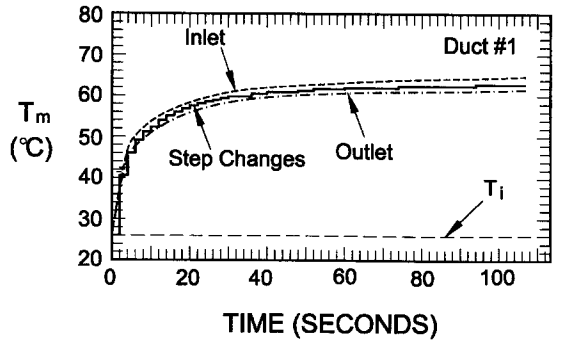

Fig. 5. Mainstream temperature history.

the test surface is valid. Noteworthy that in the region where the heat transfer coefficient varies significantly in spatiality, the heat transfer coefficient measured may be somewhat averaged by the axial conduction in the Plexiglas® plate (i.e., two- or three-dimensional effect). For checking this effect, two thermocouples are cemented into small holes drilled into the Plexiglas® plate approximately 1.0-mm in depth to measure the time-dependent axial conduction. The locations of these two thermocouples are behind the pin and ahead of the next pin, respectively, where the heat transfer is expected to be highly localized. The results show that the maximum axial conduction is less than 5% of the convection heat transfer from the fluid to the surface in the test duration.

Fig. 5 shows the typical mainstream temperature histories measured at the duct inlet and outlet. The mainstream temperature in the test section is interpolated from these two values. Since the mainstream temperature is time-dependent, the solution in Eq. 2 should be modified. First, the mainstream temperature history is simulated as a series of time step changes. Then, the time step changes of the mainstream temperature are included in the solution for the heat transfer coefficient using Duhamel's superposition theorem. The solution for the heat transfer coefficient at every location is therefore represented as

$$T_w - T_i = \sum_{j=1}^{n} \left\{ 1 - \exp\left[\frac{h^2\alpha(t-\tau_j)}{k^2}\right] \times \operatorname{erfc}\left[\frac{h\sqrt{\alpha(t-\tau_j)}}{k}\right] \right\} [\Delta T_{m(j,j-1)}] \quad (3)$$

where $\Delta T_{m(i,j-1)}$ and τ_j are the temperature and time step changes obtained from the recorder output.

2.4. Data analysis and uncertainty

The nondimensional heat transfer coefficient on the endwall of the trapezoidal duct is represented by the Nusselt number as

$$Nu = hDe/k_f \quad (4)$$

The Reynolds number used herein is based on the mean throughflow velocity at the duct entrance and the equivalent hydraulic diameter of the trapezoidal duct, i.e.,

$$Re = G \times De/\mu \quad (5)$$

Note that the above reductions of Nu and Re are similar to those in VanFossen [1], but are different from those in Metzger et al. [2], in which the Nusselt number and the Reynolds number are based on the pin diameter. This is because Metzger et al. [2] were devoted to pin-fin heat transfer, while the endwall-heat-transfer enhancement due to the pin fins in a trapezoidal duct is interested in the present study and VanFossen [1].

The pressure drop across the finite-length duct of trapezoidal cross section, either with straight or with lateral outlets, can be made dimensionless as follows [10]

$$K_L = 2\Delta P/(G^2/\rho) \quad (6)$$

The pressure-drop coefficient obtained is based on adiabatic conditions (i.e., test with ambient-temperature mainstream).

By using the estimation method of Kline and McClintock [11], the maximum uncertainties of the investigated nondimensional parameters are as follows: Re, 6.4%; Nu, 8.5%; and K_L, 7.7%. The individual contributions to the uncertainties of the nondimensional parameters for each of the measured physical properties are summarized in Table 2.

Table 2
Typical nondimensional interval for the relevant variables

Variables	Uncertainty
Air density, ρ	±1.6%
Specific heat of air, c_p	±3.0%
Dynamic viscosity of air, ν	±2.9%
Wall thermal diffusivity and conductivity, α and k	±3.0%
Equivalent duct hydraulic diameter, De	±0.5%
Air mass flux, G	±5.4%
Main stream temperature, T_m	±3.0%
Pressure difference, ΔP	±5.1%

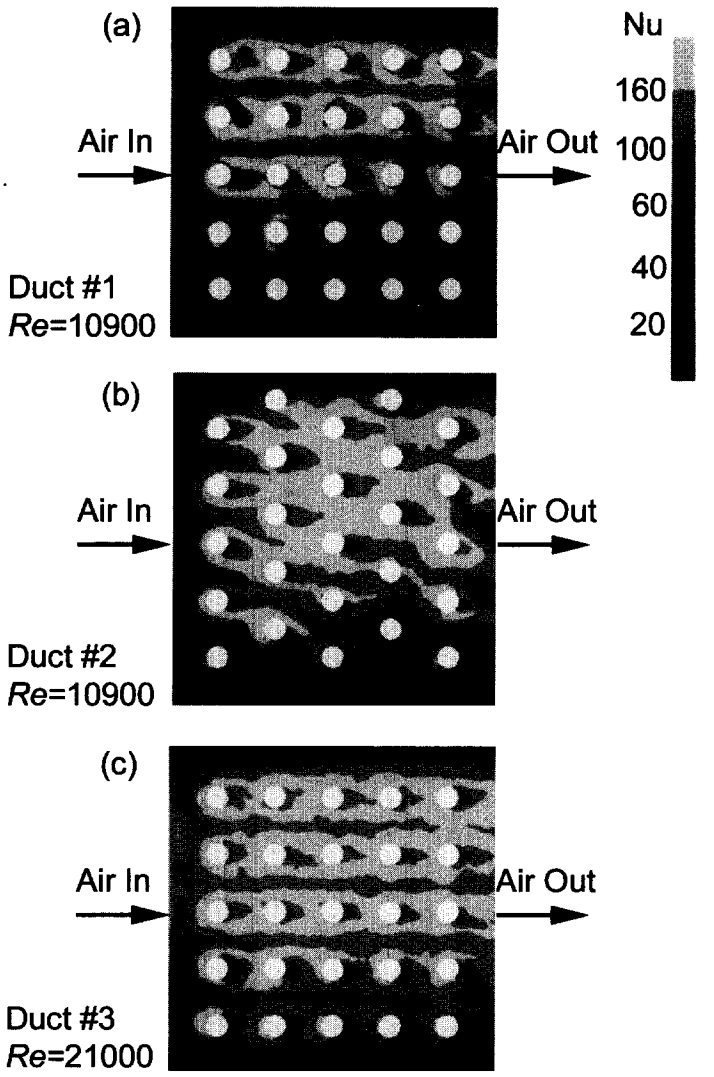

Fig. 6. Detailed heat transfer coefficient distributions for the straight trapezoidal ducts (a) duct No. 1, Re = 10,900; (b) duct No. 2, Re = 10,900; (c) duct No. 1 Re = 21,000.

3. Results and discussion

3.1. Detailed local heat transfer coefficient

Typical examples showing the detailed local Nusselt number distributions on the endwall surfaces of the trapezoidal duct under various flow and geometric conditions are given in Figs. 6 and 7. The effect of the pin arrangement on the distributions of the local heat transfer coefficient for the straight trapezoidal duct is illustrated by comparing Fig. 6(a) and (b) for a fixed Reynolds number of Re = 10,900. The flow is from left to right. The upper and lower ends of each figure represent the long and short sidewalls, respectively. The sidewall effect of the trapezoidal duct has been clearly observed from the relatively low heat transfer coefficients adjacent to the upper and lower ends of these two figures. In addition, along the spanwise direction (Y), the heat transfer coefficient is gradually decreased from the long sidewall to the short sidewall. For the in-line pin array of Fig. 6(a), the flow through the spanwise spacing between neighboring pins is similar to that in a straight channel. Such a through flow not only induces relatively low heat transfer in the region but also deposes the spanwise interactions within the array. In addition, the 'dead zones' (i.e., significantly low heat transfer coefficient) are clearly seen behind each pin. As a contrast in Fig. 6(b) for the staggered pin array, the local heat transfer coefficient distribution seems to be uniform and much higher

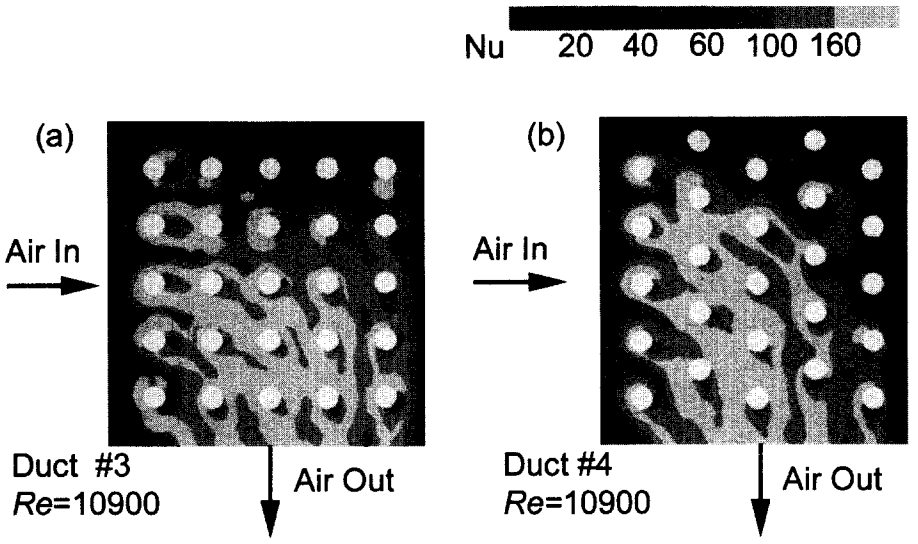

Fig. 7. Detailed heat transfer coefficient distributions for the turned trapezoidal ducts (a) duct No. 3, Re = 10,900; (b) duct No. 4, Re = 10,900.

than that in Fig. 6(a). This is because the staggered pin array introduces a significant shedding-wake effect that causes the strong flow interaction in both streamwise and spanwise directions. Moreover, the tortuous flow through the staggered pin array has improved the dead-zone heat transfer. Fig. 6(c) shows the results that the geometry is identical to that in (a) and the Reynolds number increases to Re = 21,000. It is obvious that increasing the Reynolds number has enhanced the local Nusselt number on the endwall surfaces.

Comparing the results of Figs. 6(a) and 7(a) gives an indication of the effect of outlet-flow orientation on the distributions of local heat transfer coefficient in the trapezoidal ducts with in-line pin array. Obviously, altering the outlet flow from the straight exit to the lateral exit of a trapezoidal duct has significantly enhanced the heat transfer in the region near the lateral exit (i.e., near the short side of the trapezoidal duct). This is because of the effect of the accelerating flow through the convergent lateral exit and, partly, the flow turning effect. In the region near the remote corner formed by the longer sidewall and the blocked straight exit, however, the heat transfer coefficients are degraded due to the flow recirculation. The effect of pin arrangement on the local heat transfer distributions on the endwall surfaces of the turned trapezoidal duct is shown in Fig. 7(a) and (b). In the turned trapezoidal duct, the local heat transfer seems to be insensitive to the pin arrangement investigated. Further examination of the endwall-averaged Nusselt number will be conducted later for evaluating the over-

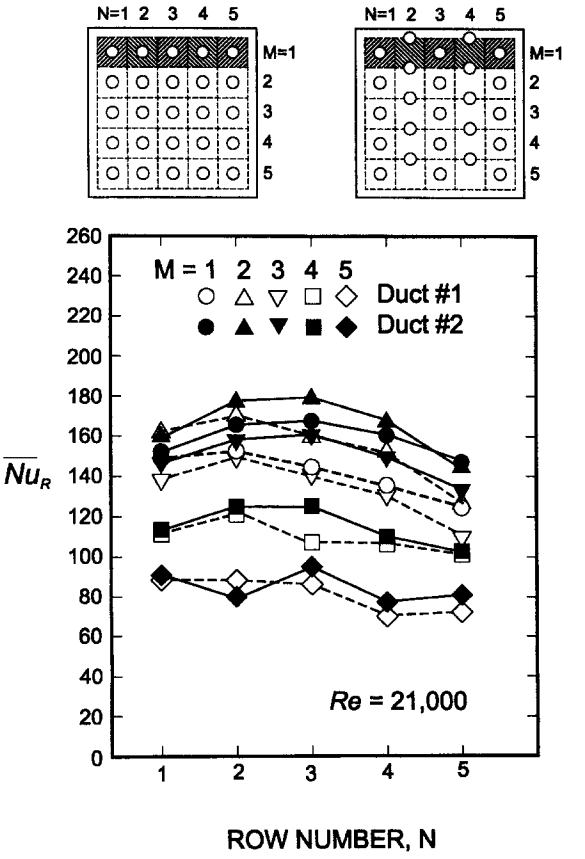

Fig. 8. Regionally averaged heat transfer distribution for the straight trapezoidal ducts.

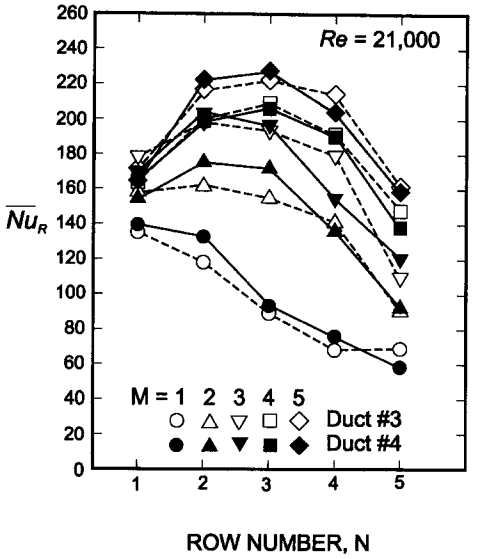

Fig. 9. Regionally averaged heat transfer distribution for the turned trapezoidal ducts.

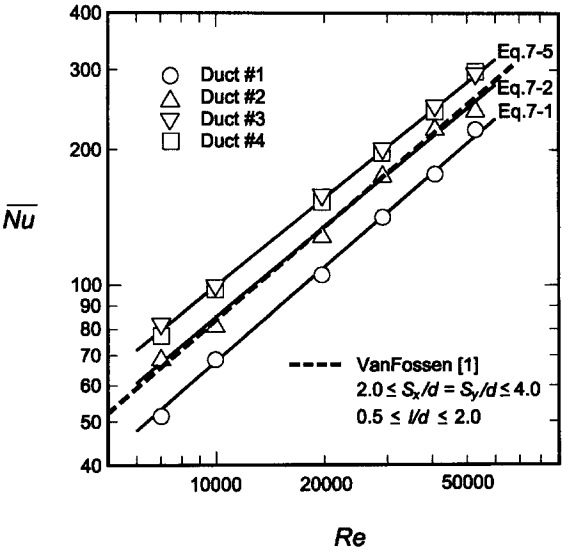

Fig. 10. Reynolds-number dependence of the endwall-averaged Nusselt number of the pin-fin trapezoidal ducts.

all heat transfer performance in trapezoidal duct of various pin configurations.

3.2. Regionally averaged Nusselt number distribution

Figs. 8 and 9 respectively present the distributions of regionally averaged Nusselt number along the X direction for the straight (duct Nos 1 and 2) and turned (duct Nos 3 and 4) trapezoidal ducts, respectively. As depicted in Fig. 8, the regionally averaged Nusselt numbers are averaged over a square area (pin location exclusive) of the endwall around a pin or between the neighboring pins. A total of 25 data points are obtained on a typical endwall. The corresponding column and row indices for each section are also provided in this figure for clarity. As given in Fig. 8, except for the region close to the short sidewall (i.e., $M = 5$), the distribution of the regionally averaged Nusselt number has a general tendency, i.e., heat transfer increases initially, reaches a peak, and then decreases downstream. The peak values occur at about the second and the third pin rows for duct Nos 1 and 2, respectively. The trend of duct No. 2 is consistent with previously reported data, for example, Metzger et al. [2]. The distributions of the row-average heat transfer are closely related to the turbulence-intensity distribution along the pin-fin channels. Metzger and Haley [3] and Simoneau and VanFossen [12] measured the turbulence intensities in rectangular channels with staggered pin array and showed an increasing-then-decreasing trend of the turbulence intensity and a peak in the turbulence level at the third pin row to the fourth pin row. As for the spanwise distribution, both the staggered and in-line pin arrays reveal that the highest and the lowest heat transfers occur at $M = 2$ and $M = 5$, respectively. In general, the staggered pin array (solid symbols) performs a better regionally average heat transfer than does the in-line pin array (open symbols).

As shown in Fig. 9, the regionally averaged heat transfer distributions for duct Nos 3 and 4 are significantly different from those for duct Nos 1 and 2. The highest heat transfer coefficients occur at the column $M = 5$, which is attributed to, as mentioned already, the effect of turning as well as accelerating lateral flow. However, near the region of the remote corner, i.e., $M = 1$ and $N = 5$, the heat transfer is largely deteriorated which is believed to be caused by the relatively slow motion of the recirculating flow.

3.3. Endwall-averaged Nusselt number

Fig. 10 shows the endwall-averaged Nusselt number as a function of the Reynolds number for the present four pin-fin trapezoidal ducts. The symbols are the actual experiments while the solid lines passing through these symbols are the curve-fitting results. In addition, the previous correlation by VanFossen [1] for pin-fin rectangular ducts is also plotted as a dashed line for comparison.

As shown in this figure, in the straight trapezoidal ducts, the staggered pin array (duct No. 2) has a higher endwall-averaged heat transfer than the in-line pin array (duct No. 1). As mentioned before, the staggered pin array produces more tortuous flow than does the in-line pin array, and hence enhances more heat transfer [13]. A comparison of the present endwall-

Table 3
Coefficients of heat transfer correlations

	$\overline{Nu} = C_1\ Re^{C_2}$			
Duct No.	C_1	C_2	Maximum error	Eq.
1	0.117	0.691	3.8%	(7-1)
2	0.187	0.666	5.3%	(7-2)
3	0.288	0.631	4.1%	(7-3)
4	0.254	0.650	4.3%	(7-4)
3 and 4	0.271	0.642	8.8%	(7-5)

averaged heat transfer coefficients of duct No. 2 and the previous results for pin-fin rectangular ducts [1] is made and shown in this figure. The trapezoidal duct No. 2 has five rows of staggered pins of an average pin length of $l/d = 2.0$, while the correlation (dashed line) was developed based on rectangular ducts with four rows of staggered pins of uniform length $l/d = 0.5$ and 2.0. Obviously, the present data are compared well with this correlation.

As for the 90° turned trapezoidal ducts (duct Nos 3 and 4), interestingly, the endwall-averaged heat transfer is nearly independent of the pin arrangements investigated. This is very reasonable because, in these two pin-fin ducts, the main flow has to turn to the lateral exit totally; in such a way, the pin array for duct No. 3 appears to be in a staggered fashion to the turning flow. That is, with respect to the turning main flow, the pin arrangements for duct Nos 3 and 4 do not differ from each other too much. Therefore, the heat transfer enhancement due to pin fins in these two ducts is almost the same. Indeed, this fact has been clearly shown in Fig. 7 for the local Nusselt number distributions.

As a collective results from the above discussion, the turned trapezoidal ducts with in-line (duct No. 3) and staggered pin arrays (duct No. 4) perform almost the same and the best endwall-averaged heat transfer, while the straight trapezoidal duct with in-line pin array (duct No. 1) has the worst endwall-averaged heat transfer. Quantitatively, turning the outlet flow laterally from the straight exit enhances the endwall-averaged heat transfer about 20 and 45% for the staggered and in-line pin arrays, respectively. As shown in Fig. 10, correlating the experimental data can obtain the following equations

$$\overline{Nu} = C_1\ Re^{C_2} \qquad (7\text{-}1)\text{–}(7\text{-}5)$$

The values of C_1 and C_2 for the four ducts investigated are listed in Table 3. The maximum deviation between the equations above and the experimental data shown in Fig. 10 is less than 5.3%. Note that when the data of duct Nos 3 and 4 are put into a single correlation of Eq. (7-5) (Table 3), the deviation will increase up to 8.8%.

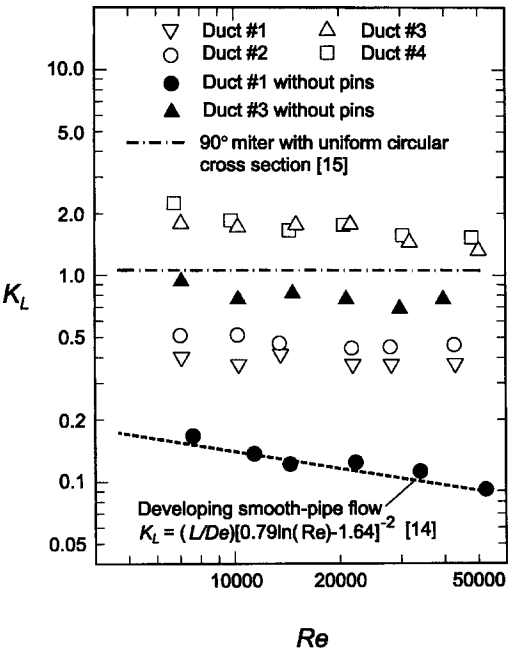

Fig. 11. Reynolds-number dependence of the pressure-drop coefficient of the pin-fin trapezoidal ducts.

3.4. Pressure-drop coefficients

The pressure drops across the present smooth as well as pin-fin trapezoidal ducts are shown in Fig. 11 as a function of Reynolds number. The solid circular and triangular symbols pertain to results of the straight and turned trapezoidal ducts without pin arrays, respectively. The dashed line is the correlation for the fully developed smooth-pipe flow [14], while the dash-dotted line represents the pressure drop across a 90° miter with uniform cross section at duct entrance and exit [15]. It is seen that the present results for the smooth trapezoidal duct with straight outlet flow are in agreement with the previous correlation [14]. This good comparison confirms the reliability of the present data and the validation of the present experimental procedure. As for the turned smooth trapezoidal duct, the pressure-drop coefficients are significantly higher than those for the straight smooth trapezoidal duct. This is because the duct with lateral outlet flow results in the separated region of the flow near the concave corner formed between the long sidewall and the blocked straight exit. In addition, a swirling secondary flow occurs due to the imbalance of the centripetal forces by reason of the curvature of the duct centerline. Both these effects increase the pressure loss

between the duct entrance and exit. It is further found that the pressure-drop coefficients of the present turned smooth trapezoidal duct are lower than those of the 90° miter [15]. This trend seems to be unexpected since the throughflow area becomes smaller and the pressure drop should become larger. Further investigation is needed to examine in detail the effect of cross-sectional area on the pressure-drop characteristics in the 90° turned duct.

When the trapezoidal ducts are inserted with pin arrays, both the pressure drops across the straight outlet duct and those across the lateral outlet duct are significantly increased. As compared with the corresponding smooth-trapezoidal duct results (solid symbols), the extension in the pressure-drop coefficient due to the pin array is about 2–3 and 3–5 times for the 90° turned trapezoidal ducts (duct Nos 3 and 4) and the straight trapezoidal ducts (duct Nos 1 and 2), respectively. Close inspection of the effect of pin arrangement shows that the staggered pin array pays more pressure-drop penalties than the in-line pin array in the straight trapezoidal duct. In the 90° turned trapezoidal duct, however, the in-line and staggered pin arrays have almost the same pressure-drop coefficients.

4. Conclusion

Endwall heat transfer coefficients and overall pressure drops in trapezoidal ducts inserted with various-length pin fins, simulating the trailing-edge cooling cavities of turbine blades, have been investigated experimentally. Four pin-fin ducts are examined in the present work. Detailed heat transfer coefficient distributions on the endwall surface are measured using a transient liquid crystal technique. The main findings based on the experiment are:

1. The heat transfer coefficient distributions on the endwall surfaces of the pin-fin trapezoidal duct are highly localized. In the straight trapezoidal duct, in general, the heat transfer coefficients are higher near the long sidewall and gradually diminish along the spanwise direction toward the short sidewall. In addition, the staggered pin array produces relatively uniform and higher heat transfer distribution than does the in-line pin array due to the stronger flow interaction in both streamwise and spanwise directions. In the 90° turned trapezoidal duct, however, the heat transfer coefficient distributions are not affected too much by the pin arrangement. They are significantly enhanced near the lateral exit, but largely deteriorated near the remote corner formed by the long sidewall and the blocked straight exit.
2. In the straight trapezoidal duct with staggered pin array, the row (regionally) averaged heat transfer distribution along the streamwise direction, except for the region close to the short sidewall, reveals that the highest heat transfer occurs at about the third pin row. This trend is consistent with previous results.
3. In the straight trapezoidal duct, the staggered pin array generally produces a much higher endwall-averaged Nusselt number than the in-line pin array, typically about 25%. Turning the outlet flow laterally from the straight exit increases the endwall-averaged heat transfer about 20 and 45% for the staggered and in-line pin arrays, respectively. Consequently, the turned trapezoidal ducts, either with the staggered pin array or with the in-line pin array, perform the best endwall-averaged heat transfer, while the straight trapezoidal duct with in-line pin array has the lowest endwall-averaged heat transfer coefficient.
4. The turned smooth trapezoidal duct has higher pressure-drop coefficients than the straight smooth trapezoidal duct. The staggered pin array pays more pressure-drop penalty as compared with the in-line pin array in a straight trapezoidal duct. In the trapezoidal duct with a lateral exit, however, the in-line and staggered pin arrays have almost the same overall pressure-drop coefficients.

Acknowledgements

This work was sponsored by the National Science Council and Taiwan Power Company of the Republic of China under contract NSC 88-TPC-E-216-003

References

[1] G.J. Vanfossen, Heat-transfer coefficients for staggered arrays of short pin fins, Trans. ASME, Journal of Heat Transfer 104 (1982) 268–274.
[2] D.E. Metzger, R.A. Berry, J.P. Bronson, Developing heat transfer in rectangular ducts with staggered pin fins, Trans. ASME, Journal of Heat Transfer 104 (1982) 700–706.
[3] D.E. Metzger, S.W. Haley Heat transfer experiments and flow visualization for arrays of short pin fins, ASME Paper No. 82-GT-138 (1982).
[4] D.E. Metzger, C.S. Fan, S.W. Haley, Effects of pin shape and array orientation on heat transfer and pressure loss in pin fin arrays, Trans. ASME, Journal of Heat Transfer 106 (1984) 252–257.
[5] B.A. Brigham, G.J. Vanfossen, Length to diameter ratio and row number effects in short pin fin heat transfer,

Trans. ASME, Journal of Engineering for Gas Turbine and Power 106 (1984) 241–245.
[6] S.C. Lau, J.C. Han, Y.S. Kim, Turbulent heat transfer and friction in pin fin channels with lateral flow injection, Trans, ASME, Journal of Heat Transfer 111 (1989) 51–58.
[7] M.K. Chyu, Heat transfer and pressure drop for short pin-fin arrays with pin-endwall, Trans. ASME, Journal of Heat Transfer 112 (1990) 926–932.
[8] J.J. Hwang, D.Y. Lai, Y.P. Tsia, Heat transfer and pressure drop in pin-fin trapezoidal ducts, Trans. ASME, Journal of Turbomachinery 121 (1999) 264–271.
[9] J.J. Hwang, C.S. Cheng, Impinged heat transfer in a triangular duct with an array of side-entry wall jets, in: Proceedings of 11th International Symposium on Transport Phenomena, 1998, pp. 244–249.
[10] J.J. Hwang, Turbulent heat transfer and fluid flow in a porous-baffled channel, AIAA, J. Thermophysics and Heat Transfer 11 (1997) 429–436.
[11] S.J. Kline, F.A. McClintock, Describing uncertainties on single-sample experiments, Mechanical Engineering 75 (1953) 3–8.
[12] R.J. Simoneau, G.J. Vanfossen, Effect of location in an array on heat transfer to a short cylinder in crossflow, Trans. ASME, J. Heat Transfer 106 (1984) 42–48.
[13] F.P. Incropera, D.P. DeWitt, Introduction to Heat Transfer, John Wiley & Sons, New York, 1994.
[14] B.S. Petukhov, in: Advances in Heat Transfer, vol. 6, Academic, New York, 1970, pp. 503–504.
[15] B.R. Munson, D.F. Young, T.H. Okiishi, Fundamentals of Fluid Mechanics, John Wiley & Sons, New York, 1994.